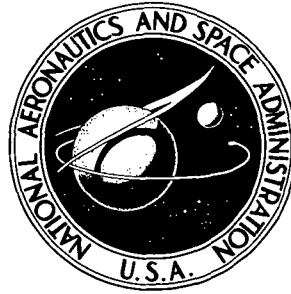NASA TECHNICAL NOTE

N73 - 24891

NASA TN D-7266

CASE FILE
COPY

THREE-DIMENSIONAL ELASTIC STRESS
AND DISPLACEMENT ANALYSIS
OF FINITE CIRCULAR GEOMETRY
SOLIDS CONTAINING CRACKS

by John P. Gyekenyesi, Alexander Mendelson,
and Jon Kring

Lewis Research Center
Cleveland, Ohio 44135

1. Report No. NASA TN D-7266	2. Government Accession No.	3. Recipient's Catalog No.
4. Title and Subtitle THREE-DIMENSIONAL ELASTIC STRESS AND DISPLACEMENT ANALYSIS OF FINITE CIRCULAR GEOMETRY SOLIDS CONTAINING CRACKS		5. Report Date May 1973
		6. Performing Organization Code
7. Author(s) John P. Gyekenyesi, Alexander Mendelson, and Jon Kring		8. Performing Organization Report No. E-7258
		10. Work Unit No. 501-21
9. Performing Organization Name and Address Lewis Research Center National Aeronautics and Space Administration Cleveland, Ohio 44135		11. Contract or Grant No.
		13. Type of Report and Period Covered Technical Note
12. Sponsoring Agency Name and Address National Aeronautics and Space Administration Washington, D.C. 20546		14. Sponsoring Agency Code

15. Supplementary Notes

16. Abstract

A seminumerical method is presented for solving a set of coupled partial differential equations subject to mixed and coupled boundary conditions. The use of this method is illustrated by obtaining solutions for two circular geometry and mixed boundary value problems in three-dimensional elasticity. Stress and displacement distributions are calculated in an axisymmetric, circular bar of finite dimensions containing a penny-shaped crack. Approximate results for an annular plate containing internal surface cracks are also presented.

17. Key Words (Suggested by Author(s)) Three-dimensional; Elasticity; Stress; Displacement; Penny-shaped crack; Stress intensity factor; Circular-geometry	18. Distribution Statement Unclassified - unlimited		
19. Security Classif. (of this report) Unclassified	20. Security Classif. (of this page) Unclassified	21. No. of Pages 46	22. Price* $3.00

CONTENTS

Page Intentionally Left Blank

THREE-DIMENSIONAL ELASTIC STRESS AND DISPLACEMENT ANALYSIS

OF FINITE CIRCULAR GEOMETRY SOLIDS CONTAINING CRACKS

by John P. Gyekenyesi, Alexander Mendelson, and Jon Kring

Lewis Research Center

SUMMARY

Displacement and stress distributions are calculated in finite circular bars, each containing a penny-shaped crack and loaded normal to the crack surface. Similar results are presented for an annular plate containing internal, traction-free surface cracks. The Navier-Cauchy equations of elastic equilibrium are reduced to three sets of coupled, simultaneous, ordinary differential equations whose solutions are obtained along sets of lines in a discretized region. Since decoupling of these equations and their boundary conditions is not possible, a successive approximation procedure is applied to obtain their analytical solution. These analytical solutions are compared with known solutions, and the results of the circular bar are used to examine the rate of convergence and the accuracy of this method. The results obtained show that the method of lines presents a systematic approach to the solution of some three-dimensional elasticity problems with arbitrary boundary conditions. The advantage of this method over other numerical solutions is that good results are obtained even from the use of a relatively coarse grid.

INTRODUCTION

The object of a problem in elasticity is usually to calculate the displacement and stress distributions in an elastic body which is subject to given body forces or surface conditions. These distributions are the solutions of the applicable field equations which mathematically model the behavior of engineering materials. The solution of this general system of equations is, however, usually too difficult to evaluate. At present, few analytical solutions of three-dimensional problems exist (ref. 1), and even these solutions frequently require symmetry conditions to simplify the governing equations. Recently, with the introduction of large digital computers, the use of a number of approx-

imate methods was attempted, but these methods yielded only partial results for these problems. Among these methods are the finite difference (ref. 2), the direct potential (ref. 3), the finite element (ref. 4), the eigenfunction expansion (ref. 5), and the line method of analysis (ref. 6). Of all these solution techniques, the line method of analysis is probably the least known and least used method in three-dimensional elasticity. Although the concept of this method for solving partial differential equations is not new (ref. 7), its useful application in the past has been limited to simple examples (ref. 8).

The line method lies midway between completely analytical and discrete methods. The basis of this solution technique is the substitution of finite differences for the derivatives with respect to all the independent variables except one, with respect to which the derivatives are retained. This approach replaces a given partial differential equation with a system of simultaneous ordinary differential equations whose solutions can then be obtained in closed form. These solutions describe the dependent variable along lines which are parallel to the coordinate in whose direction the derivatives were retained. Because of their practical importance and inherent singularities, the work in this report is concentrated on the elastic analysis of three-dimensional, finite geometry solids which contain traction-free flaws or cracks. If we assume that the method of lines can be successfully applied to these solids with inherently large stress and strain gradients, its use for less complicated elasticity problems should present little difficulty.

Early three-dimensional solutions of crack problems usually described the stresses near circular or ellipsoidal cavities enclosed in infinitely large solids. In reference 9, Sneddon applied Hankel transform methods to Love's biharmonic strain function and reduced the mixed boundary value problem of the axisymmetric half space to a set of dual integral equations. Only limited work has been done on three-dimensional solutions of crack problems in finite geometry solids. After making certain assumptions on the nature of the thickness variation of the stresses, Hartranft and Sih were successful in obtaining partial results for cracks in finite thickness bodies using variational methods (ref. 10) and eigenfunction expansions (ref. 5). In 1970, Cruse and VanBuren (ref. 11) used the direct potential method to analyze the stresses and displacements in a fracture specimen with a single edge crack.

This report presents a simple and systematic approach to the elastic analysis of three-dimensional finite and circular geometry solids which contain traction-free cracks. A discussion of the elastic solutions, obtained by the same method of lines, of similar rectangular geometry solids can be found in references 6 and 12. The advantage of this method over other numerical techniques is that good results are obtained by using relatively coarse grids. This use of a coarse grid is permissible because parts of the solutions are obtained in terms of continuous functions. Additional accuracy in normal stress distributions is derived from the fact that they are expressed as first-order derivatives of the displacements and these derivatives can be analytically evaluated. Inher-

herently inaccurate numerical differentiation is required only for the evaluation of the shear stresses, but this presents no important loss of accuracy since they are an order of magnitude smaller than the normal stresses. For problems with geometric singularities, additional accuracy is derived from using a displacement formulation since the resulting deformations are not singular.

SYMBOLS

$A(K_\rho, \rho)$	coefficient matrix of first-order differential equations, $\rho = r, \theta, z$
A_{ij}	partitioned submatrices of $e^{A\rho}$, $i = j = 1, 2$ and $\rho = \theta, z$
a	crack radius
B_i	particular integrals of first-order differential equations, $i = 1, 2, \ldots, 6$
b	outside radius
c	surface crack length emanating from internal hole
d	depth of surface crack along internal hole surface
E	Young's modulus of elasticity
e	dilatation or natural logarithm base
F_i	initial value vectors for the first-order radial differential equations, $i = 1, 2$
G	shear modulus of elasticity
h_r, h_θ, h_z	increments along cylindrical coordinate axes
I	identity matrix
K_I	stress intensity factor for opening mode
K_r, K_θ, K_z	coefficient matrices of second-order differential equations
L	half-length of cylinder
l	number of lines in radial direction
m	number of lines in circumferential direction
$NR, N\theta, NZ$	number of lines in given plane
n	number of lines in axial direction
R	distance from crack edge
r_0	internal hole radius

r, θ, z	cylindrical coordinates
$r(r)$	coupling vector for radial second-order differential equations
$s(\theta)$	coupling vector for circumferential second-order differential equations
t	half-plate thickness
$t(z)$	coupling vector for axial second-order differential equations
u	radial displacement
v	circumferential displacement
w	axial displacement
η	variable of integration
θ_0	circumferential length of annular plate cutout
λ	Lame's constant
ν	Poisson's ratio
$\left. \begin{array}{l} \sigma_r, \sigma_\theta, \sigma_z \\ \sigma_{r\theta}, \sigma_{rz}, \sigma_{\theta z} \end{array} \right\}$	components of the stress tensor in cylindrical coordinates
$\Omega_0^r(A)$	matrizant of $A(K_r, r)$
Ω_{ij}	partitioned submatrices of the matrizant of $A(K_r, r)$
∇^2	Laplacian

The symbols used in the appendixes are defined when they are introduced.

REDUCTION OF NAVIER-CAUCHY EQUATIONS TO SYSTEMS
OF ORDINARY DIFFERENTIAL EQUATIONS

The fifteen individual field equations of linearized elasticity may be combined to form the three Navier-Cauchy equations of elastic equilibrium which in cylindrical coordinates are written as

$$\frac{\partial e}{\partial r} + (1 - 2\nu)\left[\left(\nabla^2 - \frac{1}{r^2}\right)u - \frac{2}{r^2}\frac{\partial v}{\partial \theta}\right] = 0 \tag{1}$$

4

$$\frac{1}{r}\frac{\partial e}{\partial \theta} + (1 - 2\nu)\left[\left(\nabla^2 - \frac{1}{r^2}\right)v + \frac{2}{r^2}\frac{\partial u}{\partial \theta}\right] = 0 \tag{2}$$

$$\frac{\partial e}{\partial z} + (1 - 2\nu)\nabla^2 w = 0 \tag{3}$$

where the body forces are assumed to be zero and the dilatation is

$$e = \frac{\partial u}{\partial r} + \frac{1}{r}\frac{\partial v}{\partial \theta} + \frac{u}{r} + \frac{\partial w}{\partial z} \tag{4}$$

The stress-displacement relations, obtained by substituting the strain-displacement relations into Hooke's law, can be expressed in the following form:

$$\sigma_r = \lambda e + 2G\frac{\partial u}{\partial r} \tag{5}$$

$$\sigma_\theta = \lambda e + 2G\left(\frac{1}{r}\frac{\partial v}{\partial \theta} + \frac{u}{r}\right) \tag{6}$$

$$\sigma_z = \lambda e + 2G\frac{\partial w}{\partial z} \tag{7}$$

$$\sigma_{r\theta} = G\left(\frac{1}{r}\frac{\partial u}{\partial \theta} - \frac{v}{r} + \frac{\partial v}{\partial r}\right) \tag{8}$$

$$\sigma_{rz} = G\left(\frac{\partial w}{\partial r} + \frac{\partial u}{\partial z}\right) \tag{9}$$

$$\sigma_{\theta z} = G\left(\frac{\partial v}{\partial z} + \frac{1}{r}\frac{\partial w}{\partial \theta}\right) \tag{10}$$

For a finite geometry body with circular boundaries, we construct three sets of parallel lines in the direction of the coordinates as shown in figure 1. Approximate solutions of equations (1) to (3) can then be obtained by developing solutions of ordinary differential equations along the radial, circumferential, and axial lines, respectively. For equation (1), we define the displacements along the radial lines as $u_1, u_2, \ldots, u_l$. The derivatives of the circumferential displacements on these lines with respect to θ
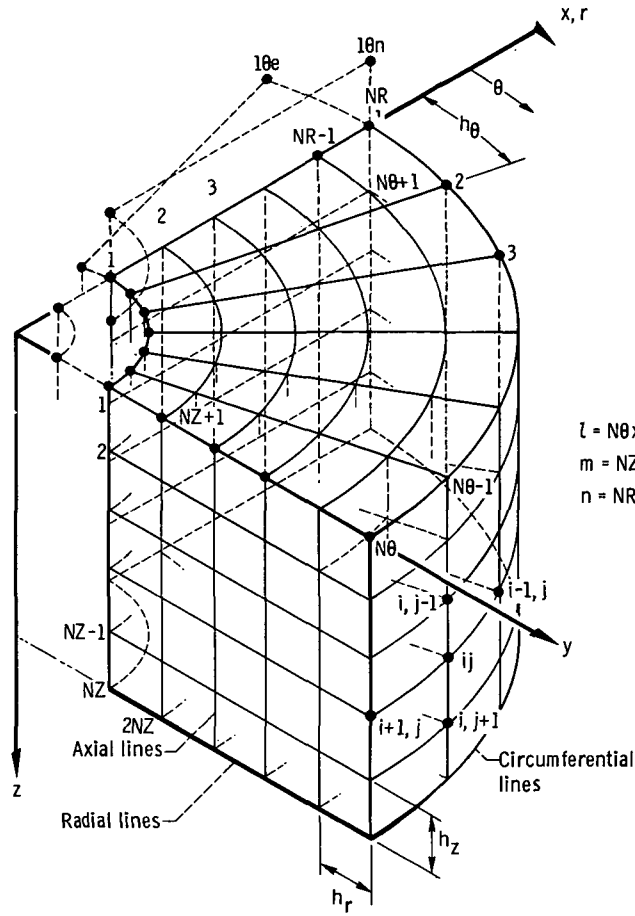
5

Figure 1. – Sets of lines in direction of cylindrical coordinates.

are defined as $\dot{v}|_1, \dot{v}|_2, \ldots, \dot{v}|_l$, and the derivatives of the axial displacements with respect to z are defined as $\dot{w}|_1, \dot{w}|_2, \ldots, \dot{w}|_l$. These displacements and derivatives can then be regarded as functions of the radius only, since they are variables on radial lines. If these definitions are used, the ordinary differential equation along a generic, radial line ij (a double subscript is used here for simplicity of writing) of figure 1 may be written as

$$\left[\frac{d^2 u_{ij}}{dr^2} + \frac{1}{r}\frac{du_{ij}}{dr} - \frac{u_{ij}}{r^2}\right] + \frac{(1 - 2\nu)}{2(1 - \nu)}\left[-\left(\frac{2}{r^2 h_\theta^2} + \frac{2}{h_z^2}\right)u_{ij} + \frac{1}{r^2 h_\theta^2}(u_{i+1,j} + u_{i-1,j})\right.$$

$$\left. + \frac{1}{h_z^2}(u_{i,j+1} + u_{i,j-1})\right] + \frac{f_{ij}(r)}{2(1 - \nu)} = 0 \quad (11)$$

6

where

$$f_{ij}(r) = \frac{(4\nu - 3)}{r^2} \dot{v}\Big|_{ij} + \frac{1}{r}\frac{d\dot{v}}{dr}\Big|_{ij} + \frac{d\dot{w}}{dr}\Big|_{ij} \qquad (12)$$

and

$$\dot{v} = \frac{dv}{d\theta}$$

$$\dot{w} = \frac{dw}{dz}$$

Similar differential equations are obtained along the other radial lines. Since each equation has the terms of the displacements on the surrounding lines, these equations constitute a system of ordinary differential equations for the displacements $u_1, u_2, \ldots, u_l$.

Noting that a second-order differential equation can satisfy only a total of two boundary conditions and since three-dimensional elasticity problems have three boundary conditions at every point of the bounding surface, some of the boundary data must be incorporated into the surface line differential equations. Hence, conditions of normal stress and displacement are enforced through the constants of the homogeneous solutions while shear stress boundary data must be incorporated into the differential equations of the surface lines. It is the application of the specified shear conditions that permits the use of central difference approximations when surface line differential equations are constructed. For the first radial line of figure 1, the use of zero shear stress boundary conditions in the radial direction on the r, z and r, θ coordinate planes gives, respectively, the following imaginary radial line displacements:

$$\left.\begin{aligned}
u_{1\theta e} &= u_2 + 2h_\theta r \frac{dv}{dr}\Big|_1 - 2h_\theta v\big|_1 \\[2mm]
u_{1\theta n} &= u_{N\theta+1} + 2h_z \frac{dw}{dr}\Big|_1
\end{aligned}\right\} \qquad (13)$$

Equations (13) must then be used in the application of central difference approximations when the ordinary differential equation for the first radial line is generated. Additional details on the construction of these equations can be found in reference 6. It is convenient to nondimensionalize these equations with respect to some characteristic dimension. Hence, we introduce the following variables:

$$\tilde{u} = \frac{u}{a} \qquad \tilde{r} = \frac{r}{a} \qquad \tilde{h}_r = \frac{h_r}{a}$$

$$\tilde{v} = \frac{v}{a} \qquad \tilde{\theta} = \theta \qquad \tilde{h}_\theta = h_\theta \qquad\qquad (14)$$

$$\tilde{w} = \frac{w}{a} \qquad \tilde{z} = \frac{z}{a} \qquad \tilde{h}_z = \frac{h_z}{a}$$

where a is the crack radius. If matrix notation is used, the differential equations along the radial lines can be expressed as

$$\left(\frac{d^2}{d\tilde{r}^2} + \frac{1}{\tilde{r}} \frac{d}{d\tilde{r}} - \frac{1}{\tilde{r}^2} \right) \tilde{u} = K_r(\tilde{r}) \ \tilde{u} + r(\tilde{r}) \qquad (15)$$

$$l \times 1 \qquad l \times l \quad l \times 1 \quad l \times 1$$

where the coefficient matrix $K_r(\tilde{r})$ is a function of the radius, the coordinate increments $\tilde{h}_\theta$ and $\tilde{h}_z$, and Poisson's ratio.

In a similar manner, for the solution of equations (2) and (3) ordinary differential equations are constructed along the circumferential and axial lines, respectively. These equations, however, are different in form from equation (15) and may be written as

$$\frac{d^2\tilde{v}}{d\tilde{\theta}^2} = K_\theta \quad \tilde{v} \quad s(\tilde{\theta}) \qquad (16)$$

$$m \times 1 \quad m \times m \ m \times 1 \ m \times 1$$

$$\frac{d^2\tilde{w}}{d\tilde{z}^2} = K_z \quad \tilde{w} + t(\tilde{z}) \qquad (17)$$

$$n \times 1 \quad n \times n \ n \times 1 \quad n \times 1$$

These two sets of equations are linear, second-order differential equations with constant coefficients. The coupling terms in each set of differential equations are grouped into the vectors $r(\tilde{r})$, $s(\tilde{\theta})$, and $t(\tilde{z})$, which are the nonhomogeneous terms in the previous equations. Since the sum of the elements in any given row of the $K_r(\tilde{r})$ and K_z coefficient matrices is zero, they are both singular. In addition, we find that K_θ is also singular, although this is not as evident from its elements as in the case of the other

coefficient matrices. A detailed listing of equations (15) to (17) may be found in reference 6.

SOLUTION OF THE SYSTEMS OF ORDINARY DIFFERENTIAL EQUATIONS

The details of a solution technique for the type of simultaneous ordinary differential equations given by equations (15) are discussed in appendix A. For the case $\tilde{r} \neq 0$, the solution vector for the radial displacement is

$$\tilde{u}(\tilde{r}) = \frac{1}{\tilde{r}} \Omega_{11}(\tilde{r}) \left[F_1 + B_1(\tilde{r}) \right] + \frac{1}{\tilde{r}} \Omega_{12}(\tilde{r}) \left[F_2 + B_2(\tilde{r}) \right] \tag{18}$$

$$l \times 1 \qquad l \times l \ \ l \times 1 \ \ l \times 1 \qquad l \times l \ \ l \times 1 \ \ l \times 1$$

where

$$F_1 = \tilde{r} \, \tilde{u} \, \bigg|_{\tilde{r} = \tilde{r}_{initial}}$$

$$F_2 = \left(\dot{\tilde{u}} + \frac{\tilde{u}}{\tilde{r}} \right)_{\tilde{r} = \tilde{r}_{initial}}$$

and $\Omega_{11}(\tilde{r})$ and $\Omega_{12}(\tilde{r})$ are infinite matrix integral series whose definitions and evaluation are discussed in appendix A. Vectors $B_1(\tilde{r})$ and $B_2(\tilde{r})$ represent particular solutions of equations (15), and they are given by

$$B_1(\tilde{r}) = - \int_{\tilde{r}_{initial}}^{\tilde{r}} \Omega_{11} \Omega_{12} \left(\Omega_{22} - \Omega_{21} \Omega_{11}^{-1} \Omega_{12} \right)^{-1} r(\eta) \, d\eta \tag{19}$$

$$B_2(\tilde{r}) = \int_{\tilde{r}_{initial}}^{\tilde{r}} \left(\Omega_{22} - \Omega_{21} \Omega_{11}^{-1} \Omega_{12} \right)^{-1} r(\eta) \, d\eta \tag{20}$$

while vectors F_1 and F_2 are initial value vectors whose evaluation from given boundary conditions is discussed in appendix C. Differentiating equation (18) with respect to $\tilde{r}$ yields

$$\dot{\tilde{u}}(\tilde{r}) = \left[\Omega_{21}(\tilde{r}) - \frac{1}{\tilde{r}^2}\Omega_{11}(\tilde{r})\right]\left[F_1 + B_1(\tilde{r})\right] + \left[\Omega_{22}(\tilde{r}) - \frac{1}{\tilde{r}^2}\Omega_{12}(\tilde{r})\right]\left[F_2 + B_2(\tilde{r})\right]$$

$$l \times 1 \qquad l \times l \qquad\quad l \times l \quad l \times 1 \quad l \times 1 \qquad l \times l \qquad\quad l \times l \quad l \times 1 \quad l \times 1$$

$$(21)$$

where $\Omega_{21}(\tilde{r})$ and $\Omega_{22}(\tilde{r})$ are matrix integral series similar to $\Omega_{11}(\tilde{r})$ and $\Omega_{12}(\tilde{r})$.

For differential equations of the type given by equations (16) and (17), a detailed and analogous solution procedure is discussed in appendix B. As a result of this development, the circumferential displacement vector may be written as

$$\tilde{v}(\tilde{\theta}) = A_{11}(\tilde{\theta})\left[\tilde{v}(0) + B_3(\tilde{\theta})\right] + A_{12}(\tilde{\theta})\left[\dot{\tilde{v}}(0) + B_4(\tilde{\theta})\right] \qquad (22)$$

where $A_{11}(\tilde{\theta})$ and $A_{12}(\tilde{\theta})$ are matrix functions:

$$A_{11}(\tilde{\theta}) = \cosh K_\theta^{1/2}\tilde{\theta} \qquad (23)$$

$$A_{12}(\tilde{\theta}) = K_\theta^{-1/2}\sinh K_\theta^{1/2}\tilde{\theta} \qquad (24)$$

The matrix $K_\theta^{1/2}$ is defined as a matrix whose square is equal to K_θ. Vectors $\tilde{v}(0)$ and $\dot{\tilde{v}}(0)$ are initial value vectors whose evaluation from given boundary conditions is discussed in appendix C. Vectors $B_3(\tilde{\theta})$ and $B_4(\tilde{\theta})$ represent particular solutions of equations (16) and are given by

$$B_3(\tilde{\theta}) = -\int_0^{\tilde{\theta}} A_{12}(\eta)s(\eta)\,d\eta \qquad (25)$$

$$B_4(\tilde{\theta}) = \int_0^{\tilde{\theta}} A_{11}(\eta)s(\eta)\,d\eta \qquad (26)$$

Differentiating equation (22) with respect to $\tilde{\theta}$ gives

$$\dot{\tilde{v}}(\tilde{\theta}) = K_\theta A_{12}(\tilde{\theta})\left[\tilde{v}(0) + B_3(\tilde{\theta})\right] + A_{11}(\tilde{\theta})\left[\dot{\tilde{v}}(0) + B_4(\tilde{\theta})\right] \qquad (27)$$

A solution vector similar to equation (22) may be constructed for equations (17) which defines the axial displacements. Since $r(\eta)$ in equations (19) and (20) is unknown, we

10

start the solution of the problem by assuming values of $\overset{.}{\tilde{v}}$, $d\overset{.}{\tilde{v}}/d\tilde{r}$, $d\overset{.}{\tilde{w}}/d\tilde{r}$, $\tilde{v}$, $d\tilde{v}/d\tilde{r}$, and $d\tilde{w}/d\tilde{r}$ along the radial lines. The initial values of these required quantities were taken to be zero in this report. Then equations (18) and (21) will give the first estimate for the vectors $\tilde{u}(\tilde{r})^{(1)}$ and $\overset{.}{\tilde{u}}(\tilde{r})^{(1)}$. It is assumed, of course, that vectors F_1 and F_2 are known or can be found from given boundary conditions. Using these calculated values of $\tilde{u}(\tilde{r})^{(1)}$ and $\overset{.}{\tilde{u}}(\tilde{r})^{(1)}$ we can evaluate the vector $\tilde{s}(\tilde{\theta})^{(1)}$ where we must use similarly assumed values of $d\overset{.}{\tilde{w}}/d\tilde{\theta}$ and $d\tilde{w}/d\tilde{\theta}$ along the circumferential lines. Equations (22) and (27) give the first values of $\tilde{v}(\tilde{\theta})^{(1)}$ and $\overset{.}{\tilde{v}}(\tilde{\theta})^{(1)}$. First values of $\tilde{w}(\tilde{z})^{(1)}$ and $\overset{.}{\tilde{w}}(\tilde{z})^{(1)}$ can then be calculated by using the first estimates of the radial and circumferential displacements and their derivatives in the coupling vector $t(\tilde{z})^{(1)}$. At this point we return to equations (18) and (21) and calculate the second values of $\tilde{u}(\tilde{r})^{(2)}$ and $\overset{.}{\tilde{u}}(\tilde{r})^{(2)}$ based on the first values of the circumferential and axial solutions.

If the values of $\tilde{u}(\tilde{r})^{(i)}$, $\overset{.}{\tilde{u}}(\tilde{r})^{(i)}$, $\tilde{v}(\tilde{\theta})^{(i)}$, $\overset{.}{\tilde{v}}(\tilde{\theta})^{(i)}$, $\tilde{w}(\tilde{z})^{(i)}$, and $\overset{.}{\tilde{w}}(\tilde{z})^{(i)}$ converge with the repetition of this procedure, an approximate solution of a given problem will be determined. In general, the convergence rate for these successive calculations is dependent on the accuracy to which the matrix functions A_{ij} and the matrix integral series Ω_{ij} can be evaluated. Sufficiently large errors in these matrix variables will lead to divergence in the successive approximation calculations.

Since the coupling vectors $r(\tilde{r})$, $s(\tilde{\theta})$, and $t(\tilde{z})$ involve displacements and their derivatives defined only at the nodes, finite difference calculus must be used in evaluating their elements. Hence, all the particular integrals are calculated by a suitable numerical integration technique.

Once the displacement field in the bar has been calculated and the successive approximation procedure has converged, the normal stress distributions along the three sets of parallel lines can be obtained from

$$\sigma_r = (\lambda + 2G)(\overset{.}{\tilde{u}})_{\substack{\text{Along radial} \\ \text{lines}}} + \lambda\left(\frac{\tilde{u}}{\tilde{r}} + \frac{1}{\tilde{r}}\overset{.}{\tilde{v}} + \overset{.}{\tilde{w}}\right)_{\substack{\text{Along radial} \\ \text{lines}}} \tag{28}$$

$$\sigma_\theta = (\lambda + 2G)\left(\frac{\overset{.}{\tilde{v}}}{\tilde{r}} + \frac{\tilde{u}}{\tilde{r}}\right)_{\substack{\text{Along circumfer-} \\ \text{ential lines}}} + \lambda(\overset{.}{\tilde{u}} + \overset{.}{\tilde{w}})_{\substack{\text{Along circumfer-} \\ \text{ential lines}}} \tag{29}$$

$$\sigma_z = (\lambda + 2G)(\overset{.}{\tilde{w}})_{\substack{\text{Along axial} \\ \text{lines}}} + \lambda\left(\overset{.}{\tilde{u}} + \frac{\tilde{u}}{\tilde{r}} + \frac{\overset{.}{\tilde{v}}}{\tilde{r}}\right)_{\substack{\text{Along axial} \\ \text{lines}}} \tag{30}$$

Note that these equations involve only derivatives that can be analytically evaluated. The shear stresses at each node can be calculated from equations (8) to (10), but finite difference approximations must be used for the required displacement gradients.

NUMERICAL RESULTS

Solid Cylindrical Bar with Penny-Shaped Crack

Figure 2 shows a cylindrical bar containing a penny-shaped crack and loaded by a uniform normal stress distribution. For problems with axisymmetric geometry, the circumferential displacement is inherently zero at every point and all the remaining variables are independent of the circumferential coordinate θ. The two sets of parallel
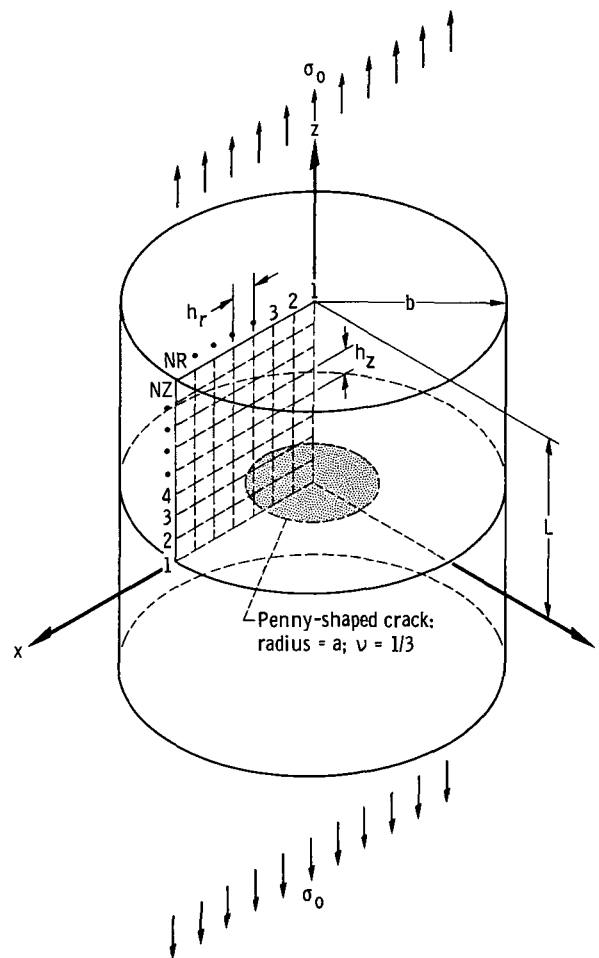

Figure 2. - Solid cylindrical bar with penny-shaped crack.

lines needed for the solution of this problem are also shown in this figure. Note that the crack edge is assumed to be midway between adjacent nodes, specifying normal stress and displacement boundary conditions, respectively.

The solution of this problem was obtained by using two different sets of lines along the coordinate axes so that the convergence of the finite difference approximations could be checked. The successive approximation procedure required for decoupling the two sets of ordinary differential equations was terminated when the difference between suc-cessively calculated displacements at every point was less than a preset value (10^{-6}). Selected results from these calculations are shown in tables I to V and figures 3 to 7. For easy comparison of data, some of these figures include Sneddon's results for an

TABLE I. - NONDIMENSIONALIZED RADIAL DISPLACEMENTS $Eu/\sigma_0 a$

FOR SOLID CYLINDRICAL BAR WITH PENNY-SHAPED CRACK

UNDER UNIFORM NORMAL TENSION

$[\tilde{a} = 1.0, \tilde{b} = 1.77, \tilde{L} = 1.68$ (16 axial and 13 radial lines).$]$

$\tilde{z}$	$\tilde{r}$								
	0.000	0.235	0.471	0.706	0.941	1.06	1.294	1.530	1.770
0.00	0.000	-0.168	-0.333	-0.488	-0.579	-0.609	-0.653	-0.705	-0.773
.28		-.080	-.153	-.217	-.297	-.371	-.529	-.639	-.725
.56		-.045	-.091	-.149	-.239	-.300	-.433	-.549	-.646
.84		-.038	-.083	-.142	-.223	-.273	-.379	-.482	-.580
1.12		-.039	-.085	-.142	-.214	-.255	-.344	-.435	-.530
1.40		-.034	-.074	-.124	-.188	-.224	-.303	-.388	-.483
1.68		-.006	-.023	-.058	-.114	-.150	-.233	-.325	-.425

infinite solid (ref. 9). The data of figure 3 clearly show the advantage of the line method over other numerical solutions. A relatively coarse grid of nine axial and nine radial lines gave almost identical results to those obtained by using a 16 by 13 grid. Since the bar is of finite size, the crack opening displacement is expected to be higher than Sneddon's solution. Consistency of the results with this conclusion is obvious from figure 6. It is noteworthy that the results correspond to elliptical crack profiles in all cases. The maximum dimensionless crack opening is plotted for several crack to cyl-inder radius ratios in figure 7. The data from figure 6 match the results of Sneddon and Welch (ref. 13) very closely, and, as expected, the maximum crack opening is slightly higher for finite length cylinders.

Figure 5 shows the stress distribution normal to the crack plane as a function of the distance from the crack edge. As shown by Sneddon for an infinite solid, this stress

13

TABLE II. - NONDIMENSIONALIZED AXIAL DISPLACEMENTS

$Ew/\sigma_0 a$ FOR SOLID CYLINDRICAL BAR WITH

PENNY-SHAPED CRACK UNDER

UNIFORM NORMAL TENSION

[$\tilde{a}$ = 1.0, $\tilde{b}$ = 1.77, $\tilde{L}$ = 1.68 (16 axial and 13 radial lines).]

$\tilde{r}$	$\tilde{z}$						
	0.000	0.280	0.560	0.840	1.120	1.400	1.680
0.000	1.394	1.544	1.646	1.766	1.928	2.126	2.329
.235	1.351	1.495	1.595	1.722	1.892	2.097	2.306
.471	1.219	1.359	1.472	1.622	1.812	2.029	2.250
.706	.973	1.113	1.273	1.473	1.696	1.933	2.167
.941	.515	.746	1.029	1.302	1.565	1.823	2.072
1.060	.000	.542	.913	1.221	1.502	1.768	2.024
1.294	↓	.384	.758	1.090	1.390	1.670	1.937
1.530		.334	.673	.999	1.304	1.592	1.866
1.770		.291	.610	.935	1.245	1.535	1.812

TABLE III. - NONDIMENSIONALIZED RADIAL STRESS σ_r/σ_0 FOR

SOLID CYLINDRICAL BAR WITH PENNY-SHAPED CRACK

UNDER UNIFORM NORMAL TENSION

[$\tilde{a}$ = 1.0, $\tilde{b}$ = 1.77, $\tilde{L}$ = 1.68 (16 axial and 13 radial lines).]

$\tilde{z}$	$\tilde{r}$								
	0.000	0.235	0.471	0.706	0.941	1.060	1.244	1.530	1.770
0.00	-1.060	-1.043	-1.017	-0.883	-0.522	1.134	0.376	0.116	0.000
.28	-.479	-.451	-.375	-.270	-.262	-.138	-.095	-.017	↓
.56	-.148	-.141	-.123	-.124	-.155	-.150	-.113	-.044	
.84	.0211	.0144	.002	-.0251	-.058	-.065	-.056	-.026	
1.12	.127	.116	.093	.058	.023	.009	-.004	-.003	
1.40	.246	.230	.193	.142	.088	.064	.028	.012	
1.68	.470	.429	.352	.247	.136	.085	.008	-.021	↓

TABLE IV. - NONDIMENSIONALIZED CIRCUMFERENTIAL STRESS σ_θ/σ_0

FOR SOLID CYLINDRICAL BAR WITH PENNY-SHAPED CRACK

UNDER UNIFORM NORMAL TENSION

$[\tilde{a} = 1.0, \ \tilde{b} = 1.77, \ \tilde{L} = 1.68$ (16 axial and 13 radial lines).$]$

$\tilde{z}$	$\tilde{r}$								
	0.000	0.235	0.471	0.706	0.941	1.060	1.294	1.530	1.770
0.00	-1.060	-1.061	-1.047	-0.986	-0.790	0.909	0.125	-0.020	-0.108
.28	-.479	-.461	-.401	-.291	-.112	.108	.015	-.023	-.051
.56	-.148	-.138	-.106	-.055	.011	.049	.037	.022	.024
.84	.021	.023	.032	.047	.062	.067	.062	.055	.057
1.12	.127	.124	.120	.113	.104	.099	.086	.075	.064
1.40	.246	.23	.218	.191	.160	.144	.116	.096	.072
1.68	.470	.45	.401	.333	.257	.220	.154	.112	.089

TABLE V. - NONDIMENSIONALIZED AXIAL STRESS σ_z/σ_0 FOR

SOLID CYLINDRICAL BAR WITH PENNY-SHAPED CRACK

UNDER UNIFORM NORMAL TENSION

$[\tilde{a} = 1.0, \ \tilde{b} = 1.77, \ \tilde{L} = 1.68$ (16 axial and 13 radial lines).$]$

$\tilde{z}$	$\tilde{r}$								
	0.000	0.235	0.471	0.706	0.941	1.060	1.294	1.530	1.770
0.00	0.000	0.000	0.000	0.000	0.000	3.320	1.512	1.206	0.989
.28	.095	.093	.146	.319	.874	1.513	1.365	1.201	1.082
.56	.277	.295	.386	.592	.950	1.150	1.230	1.186	1.172
.84	.515	.542	.624	.770	.957	1.041	1.122	1.136	1.159
1.12	.736	.759	.808	.885	.972	1.010	1.059	1.082	1.092
1.40	.900	.915	.933	.960	.990	1.003	1.022	1.036	1.037
1.68	.999	.998	.999	.999	1.000	.999	.995	.993	.990

(a) Dimensionless axial displacement distribution (16 by 13 grid).

$\tilde{a} = 1.0$ $\nu = 1/3$
$\tilde{b} = 1.77$ $\tilde{h}_r = 0.1176$
$\tilde{L} = 1.68$ $\tilde{h}_z = 0.140$

(b) Dimensionless axial displacement distribution (9 by 9 grid).

$\tilde{a} = 1.0$ $\nu = 1/3$
$\tilde{b} = 1.77$ $\tilde{h}_r = 0.222$
$\tilde{L} = 1.68$ $\tilde{h}_z = 0.210$
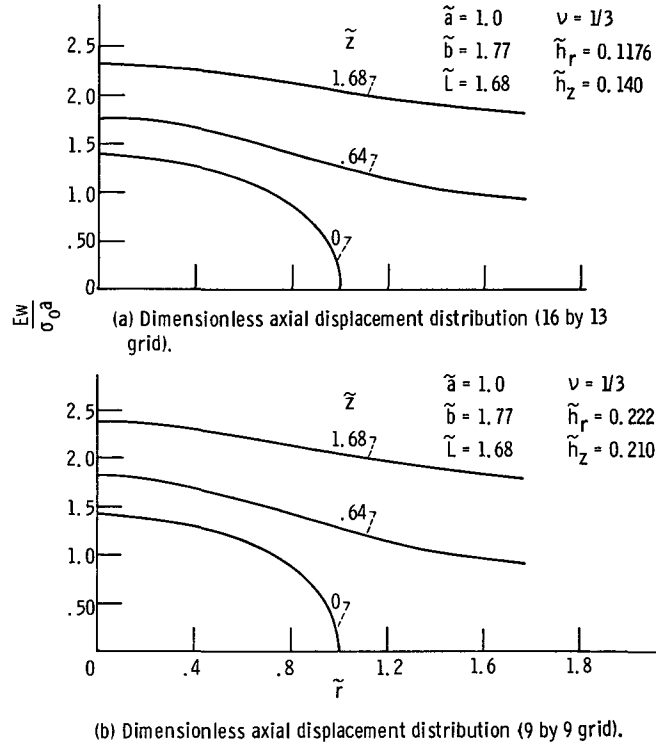
Figure 3. - Dimensionless axial displacement distribution
for solid cylindrical bar with penny-shaped crack.

distribution should approach infinity near the crack edge as the inverse square root of
the distance from the crack edge. Establishment of this type of singularity is, however,
difficult when numerical methods are used because values of the normal stress are
needed within a distance of 0.05 a or less from the crack tip. For the range of $\tilde{r}$
shown in figure 5, this inverse square root singularity is not defined. However, for the
range shown, the obtained stress curve closely resembles Sneddon's solution (ref. 15).
As expected, the absolute value of this stress is greater for a finite size bar than for
Sneddon's infinite solid. Tables I to V show selected results from the computer listings.
The accuracy of the normal stress and displacement boundary conditions can easily be
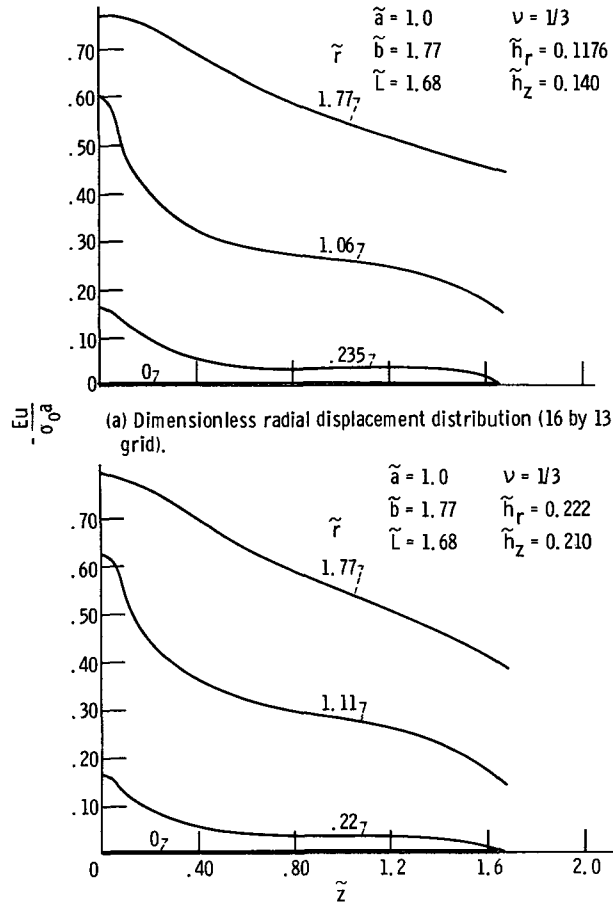noted from the numerical data listed.

16

$-\dfrac{Eu}{\sigma_0 a}$

(a) Dimensionless radial displacement distribution (16 by 13 grid).

(b) Dimensionless radial displacement distribution (9 by 9 grid).

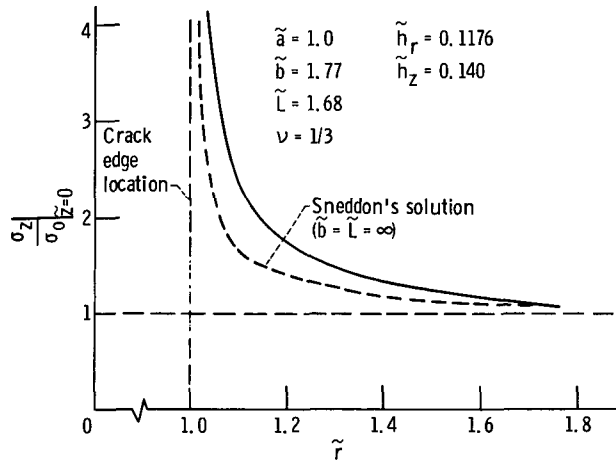Figure 4. – Dimensionless radial displacement distribution for solid cylindrical bar with penny-shaped crack.

Figure 5. – Dimensionless axial stress distribution (16 by 13 grid) for solid cylindrical bar with penny-shaped crack at $\tilde{z} = 0$.
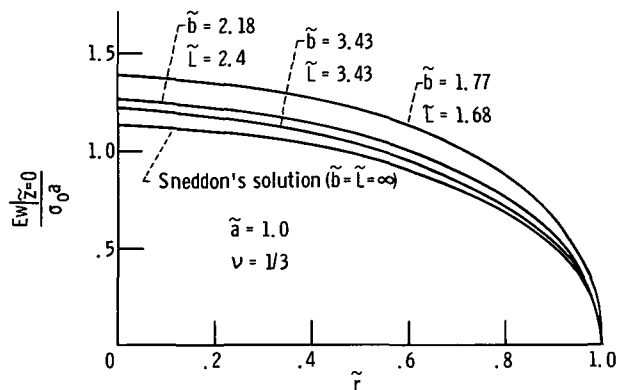
Figure 6. – Dimensionless crack opening displacements for solid cylindrical bars with penny-shaped cracks of various lengths and radii.
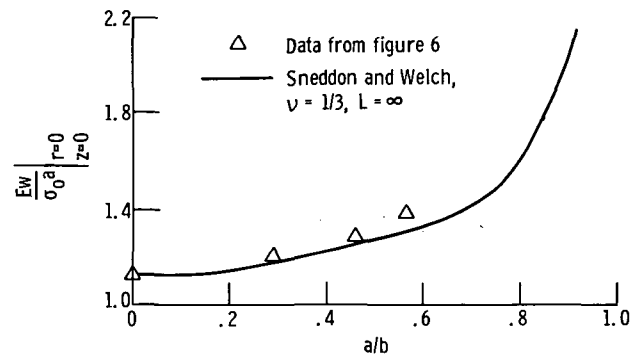
Figure 7. – Dimensionless maximum crack opening as function of crack to cylinder radius ratio.

Annular Plate with Internal Surface Cracks

As a first attempt at the solution of a general three-dimensional problem in cylindrical coordinates, the problem of figure 8 was investigated. In order to minimize the numerical computations, we have assumed four symmetrically located internal surface cracks. Because of the symmetric geometry and loading, only one-sixteenth of the original plate has to be discretized. Figure 9 shows this region of interest and the assumed crack geometry. Note that nondimensionalization with respect to the outside radius is more convenient in this case since the crack has two characteristic dimensions.

Displacement and normal stress distributions were calculated along the lines of figure 9 using a grid of 16 lines in all directions. Because of the relatively coarse grid involved, the results appear only in tabular form (tables VI to XI). It must be noted, however, that because of the unknown nature of the resulting solutions, the use of a coarse grid is always recommended in generating the first set of displacements. Since the construction of a general computer program for this problem requires a great amount of effort, the results in tables VI to XI were calculated by using only one set of lines with $NR = N\theta = NZ = 4$.

Tables VI to VIII contain the dimensionless displacement distributions. These results show that below the crack plane the circumferential displacements are essentially zero while the maximum crack opening is at $\tilde{\theta} = \tilde{z} = 0$ and $\tilde{r} = 0.25$. Although both radial and circumferential displacement fields are extensional, the axial displacements are negative, which indicates a contraction in that direction. The calculated normal
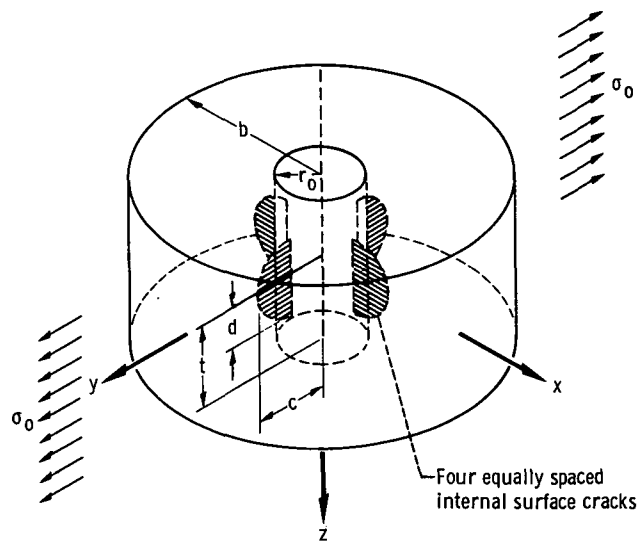
18

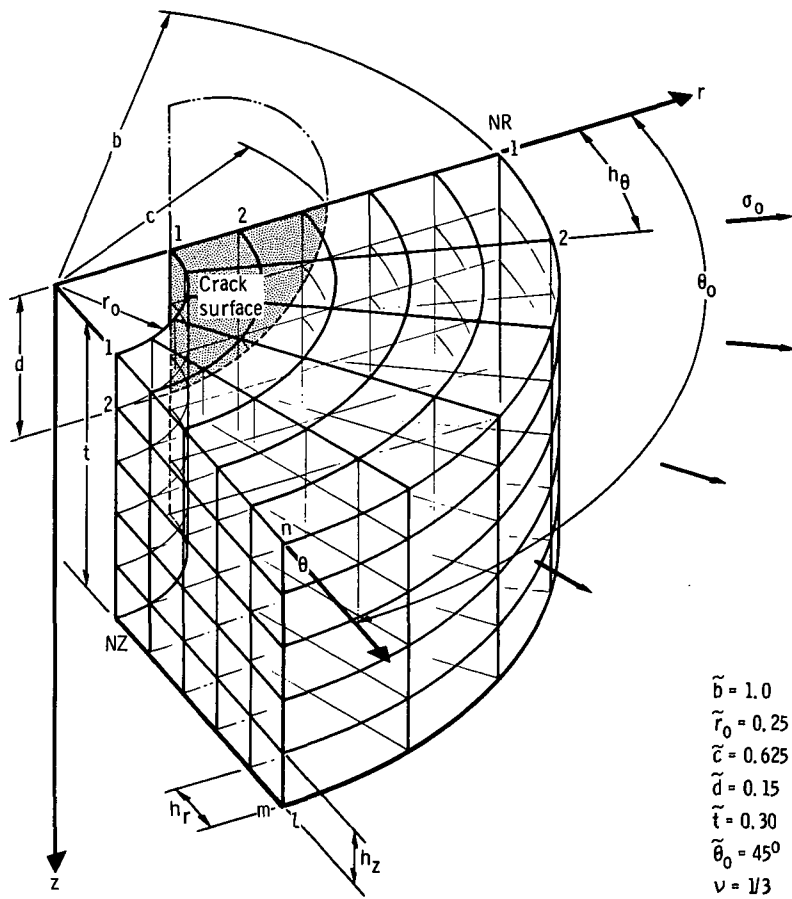Figure 8. – Annular plate with internal surface cracks under uniform external tension.

$\tilde{b} = 1.0$

$\tilde{r}_0 = 0.25$

$\tilde{c} = 0.625$

$\tilde{d} = 0.15$

$\tilde{t} = 0.30$

$\tilde{\theta}_0 = 45^0$

$\nu = 1/3$

Figure 9. – Part of annular plate with internal surface cracks.

19

TABLE VI. - DIMENSIONLESS RADIAL DISPLACEMENTS

$Eu/\sigma_{0}b$ FOR ANNULAR PLATE WITH INTERNAL

SURFACE CRACKS UNDER UNIFORM RADIAL

TENSION ON OUTSIDE SURFACE

$\tilde{\theta}$, deg	$\tilde{r}$			
	0.25	0.50	0.75	1.00
$\tilde{z} = 0.00$				
0	0.435	0.671	0.786	0.930
15	.940	.890	.896	.998
30	.168	.992	.968	1.058
45	1.240	1.026	.994	1.081
$\tilde{z} = 0.10$				
0	0.506	0.680	0.789	0.930
15	.907	.860	.886	.994
30	1.092	.953	.957	1.055
45	1.152	.986	.984	1.076
$\tilde{z} = 0.20$				
0	0.724	0.656	0.779	0.927
15	.795	.761	.856	.965
30	.898	.856	.932	1.048
45	.942	.892	.961	1.073
$\tilde{z} = 0.30$				
0	0.716	0.659	0.769	0.915
15	.752	.727	.845	.978
30	.815	.809	.926	1.049
45	.845	.843	.957	1.077

TABLE VII. - DIMENSIONLESS CIRCUMFERENTIAL

DISPLACEMENTS $Ev/\sigma_0 b$ FOR ANNULAR PLATE

WITH INTERNAL SURFACE CRACKS UNDER

UNIFORM RADIAL TENSION ON

OUTSIDE SURFACE

$\tilde{z}$	$\tilde{\theta}$, deg			
	0	15	30	45
$\tilde{r} = 0.25$				
0.00	0.718	0.566	0.302	0.000
.10	.592	.450	.238	↓
.20	.000	.073	.063	
.30	.000	.009	.012	
$\tilde{r} = 0.50$				
0.00	0.425	0.285	0.138	0.000
.10	.350	.232	.115	↓
.20	.000	.075	.057	
.30	.000	.023	.026	
$\tilde{r} = 0.75$				
0.00	0.000	0.037	0.029	0.000
.10	↓	.033	.026	↓
.20		.023	.020	
.30		.014	.014	
$\tilde{r} = 1.00$				
0.00	0.000	0.006	0.004	0.000
.10	↓	.007	.005	↓
.20		.009	.007	
.30		.010	.007	

TABLE VIII. - DIMENSIONLESS AXIAL DISPLACEMENTS

$Ew/\sigma_o b$ FOR ANNULAR PLATE WITH INTERNAL

SURFACE CRACKS UNDER UNIFORM RADIAL

TENSION ON OUTSIDE SURFACE

$\tilde{r}$	$\tilde{z}$			
	0.00	0.10	0.20	0.30
$\tilde{\theta} = 0^{\circ}$				
0.25	0.000	-0.218	-0.342	-0.416
.50		-.108	-.217	-.322
.75		-.089	-.175	-.256
1.00	↓	-.076	-.152	-.226
$\tilde{\theta} = 15^{\circ}$				
0.25	0.000	-0.098	-0.216	-0.336
.50		-.049	-.131	-.232
.75		-.075	-.154	-.237
1.00	↓	-.074	-.149	-.226
$\tilde{\theta} = 30^{\circ}$				
0.25	0.000	-0.068	-0.167	-0.281
.50		-.040	-.106	-.195
.75		-.067	-.141	-.222
1.00	↓	-.075	-.152	-.231
$\tilde{\theta} = 45^{\circ}$				
0.25	0.000	-0.061	-0.153	-0.262
.50		-.039	-.101	-.186
.75		-.065	-.137	-.218
1.00	↓	-.075	-.153	-.233

TABLE IX. - DIMENSIONLESS RADIAL STRESS

DISTRIBUTION σ_r/σ_o FOR ANNULAR

PLATE WITH INTERNAL SURFACE

CRACKS UNDER UNIFORM

RADIAL TENSION ON

OUTSIDE SURFACE

$\tilde{\theta}$, deg	$\tilde{r}$			
	0.25	0.50	0.75	1.00
$\tilde{z} = 0.00$				
0	0.000	0.020	1.062	1.000
15		.346	.837	
30		.293	.748	
45		.282	.726	
$\tilde{z} = 0.20$				
0	0.000	0.027	1.048	1.000
15		.405	.872	
30		.424	.801	
45		.424	.783	
$\tilde{z} = 0.10$				
0	0.000	1.305	1.026	1.000
15		.968	.980	
30		.840	.932	
45		.801	.915	
$\tilde{z} = 0.30$				
0	0.000	0.872	1.005	1.000
15		.950	1.004	
30		.966	.986	
45		.956	.975	

TABLE X. - DIMENSIONLESS CIRCUMFERENTIAL

STRESS σ_θ/σ_0 FOR ANNULAR PLATE WITH

INTERNAL SURFACE CRACKS UNDER

UNIFORM RADIAL TENSION ON

OUTSIDE SURFACE

$\tilde{\theta}$, deg	$\tilde{r}$			
	0.25	0.50	0.75	1.00
$\tilde{z} = 0.00$				
0	0.000	0.000	1.702	1.251
15	.308	.803	1.542	1.339
30	.209	1.043	1.460	1.416
45	.240	1.145	1.441	1.443
$\tilde{z} = 0.10$				
0	0.000	0.000	1.659	1.246
15	.703	.957	1.534	1.331
30	.803	1.196	1.472	1.410
45	.863	1.270	1.456	1.439
$\tilde{z} = 0.20$				
0	4.569	2.821	1.506	1.236
15	3.609	2.011	1.526	1.313
30	2.971	1.706	1.506	1.400
45	2.748	1.629	1.498	1.432
$\tilde{z} = 0.30$				
0	3.050	1.858	1.442	1.220
15	3.110	1.879	1.500	1.301
30	3.171	1.825	1.523	1.397
45	3.167	1.775	1.524	1.432

TABLE XI. - DIMENSIONLESS AXIAL STRESS σ_z/σ_o

FOR ANNULAR PLATE WITH INTERNAL SURFACE

CRACKS UNDER UNIFORM RADIAL TENSION

ON OUTSIDE SURFACE

$\tilde{\theta}$, deg	$\tilde{r}$			
	0.25	0.50	0.75	1.00
$\tilde{z} = 0.00$				
0	-1.974	-1.049	0.030	-0.014
15	-.939	-.126	.043	.040
30	-.631	.041	.064	.060
45	-.544	.082	.070	.062
$\tilde{z} = 0.10$				
0	-1.597	-1.073	0.028	-0.010
15	-.867	-.210	.032	.031
30	-.579	.006	.053	.046
45	-.487	.055	.059	.048
$\tilde{z} = 0.20$				
0	0.500	0.313	0.002	-0.004
15	-3.135	-1.996	-1.504	-1.310
30	-.077	.070	.039	.019
45	-.097	.073	.042	.020
$\tilde{z} = 0.30$				
0	0.000	0.000	0.000	0.000
15	↓	↓	↓	↓
30				
45				

stresses are summarized in tables IX to XI. It is expected that the circumferential stress be the maximum tensile stress in the body since the crack plane is normal to this coordinate. The interaction between the hole and crack stress fields should also be most pronounced at the inside radius; from this we conclude that the stress should be maximum at that point. The results of table X seem to confirm these observations, although we must also remember that the nodes are closer to the crack boundary below the crack surface than along the radius.

Because of the use of a coarse grid, the numerical results for this example are somewhat inaccurate in magnitude but they do indicate some previously unknown variations in the stress field for this problem. This conclusion is possible in that the line method does not usually require a fine grid for good results as was shown in the previous section. These results also demonstrate that the method of lines permits the computation of the displacement and stress fields for a general three-dimensional problem.

STRESS INTENSITY FACTOR

It is customary in fracture mechanics to describe the plane elasticity crack opening displacement as a superposition of three basic deformation modes (ref. 14). In terms of the stress intensity factor for the opening mode K_I, the plane elasticity crack displacements near the crack tip are given by (ref. 14)

$$v\big|_{y=0} = \frac{2(1 - \nu)}{G} K_I \sqrt{\frac{R}{2\pi}} \qquad \text{plane strain} \tag{31}$$

$$v\big|_{y=0} = \frac{2}{(1 + \nu)G} K_I \sqrt{\frac{R}{2\pi}} \qquad \text{plane stress} \tag{32}$$

Since three-dimensional problems are neither in a state of plane strain nor plane stress, the definition of a stress intensity factor for these problems must be first established. The problem we consider in detail is Sneddon's penny-shaped crack solution. Reference 15 gives the crack opening displacement as

$$w\big|_{z=0} = \frac{4\sigma_0(1 - \nu^2)}{\pi E} \sqrt{a^2 - r^2} \tag{33}$$

which for small values of R, where R = a - r, becomes

26

$$w\Big|_{z=0} = \frac{4\sigma_0(1 - \nu^2)}{\pi E}\sqrt{2aR} \tag{34}$$

Note that adjustment of coordinates must be made between the equations quoted from references 14 and 15. Paris and Sih (ref. 14) list the stress intensity factor for this problem as

$$K_I = \frac{2}{\sqrt{\pi}}\sigma_0\sqrt{a} \tag{35}$$

In terms of this stress intensity factor, the crack opening displacement (eq. (34)) becomes

$$w\Big|_{z=0} = K_I\frac{2(1 - \nu^2)}{E}\sqrt{\frac{2R}{\pi}} = \frac{2(1 - \nu)}{G}K_I\sqrt{\frac{R}{2\pi}} \tag{36}$$

Rearranging this equation in terms of the known dimensionless displacements $(E/\sigma_0)(w/a)\Big|_{z=0}$ gives

$$\frac{E}{\sigma_0}C_IK_I = \frac{\dfrac{E}{\sigma_0}\dfrac{w}{a}\Big|_{z=0}}{\sqrt{\dfrac{R}{a}}} \tag{37}$$

where

$$C_I = \frac{4(1 - \nu^2)}{E\sqrt{2\pi a}} \tag{38}$$

Then a plot of equation (37) as $\sqrt{R/a} \rightarrow 0$ gives the desired value of $(E/\sigma_0)C_IK_I$ from which an equivalent stress intensity factor for finite geometry cylinders can be calculated. Note from equation (36) that the definition of K_I given in equation (35) implies the plane strain crack opening displacement of equation (31).

For problems in which the crack opening displacement varies in the thickness direction, such as the annular plate with internal surface cracks, the stress intensity factor obtained previously will be a function of the thickness variable. However, if we were to account for the nonplane strain conditions near the surface by using equation (32) or a

corrected equation (31) for the definition of K_I, the stress intensity factor would become a constant across the thickness by definition. It should be noted that this description of K_I is completely arbitrary and its significance in three-dimensional elasticity theory is of doubtful value. However, values of K_I are still presented so that a comparison will be possible between the calculated results and the published plane strain solutions (ref. 14).

Figure 10 contains the calculation of K_I according to equation (37) for the penny-shaped crack problems. The value of K_I calculated from Sneddon's solution agrees
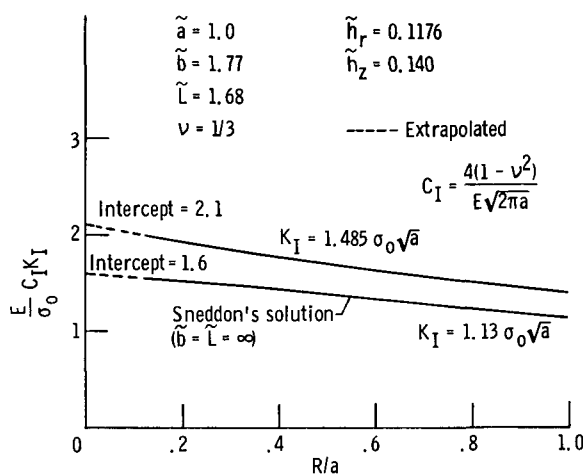
Figure 10. – Calculation of the stress intensity factor K_I for a solid cylindrical bar with a penny shaped crack (16 by 13 grid).

with equation (35), while for the finite size bar we obtain a value of K_I equal to 1.485 $\sigma_0 \sqrt{a}$. Hence, the finite bar discussed in figure 10 has an approximately 31 percent higher stress intensity factor than the infinite solid.

Lewis Research Center,
   National Aeronautics and Space Administration,
      Cleveland, Ohio, February 22, 1973,
         501-21.

28

APPENDIX A

SOLUTION OF SIMULTANEOUS DIFFERENTIAL EQUATIONS

WITH VARIABLE COEFFICIENTS

Noting that the differential operator of equations (15) can be written as $d/d\tilde{r}\left[1/\tilde{r} \times d/d\tilde{r} (\tilde{r} u)\right]$, the following variables are introduced in order to obtain a system of first-order differential equations:

$$U_1 = \tilde{r}\,\tilde{u}_1, \ U_2 = \tilde{r}\,\tilde{u}_2, \ \ldots, \ U_l = \tilde{r}\,\tilde{u}_l$$

$$U_{l+1} = \frac{1}{\tilde{r}}\frac{1}{d\tilde{r}}(\tilde{r}\,\tilde{u}_1), \ U_{l+2} = \frac{1}{\tilde{r}}\frac{d}{d\tilde{r}}(\tilde{r}\,\tilde{u}_2), \ \ldots, \ U_{2l} = \frac{1}{\tilde{r}}\frac{d}{d\tilde{r}}(\tilde{r}\,\tilde{u}_l) \tag{A1}$$

In terms of these variables, equations (15) can be written as

$$\underset{2l\times 1}{\frac{dU}{d\tilde{r}}} = \underset{2l\times 2l}{A(\tilde{r})} \quad \underset{2l\times 1}{U} \quad \underset{2l\times 1}{\bar{r}(\tilde{r})} \tag{A2}$$

where

$$\underset{2l\times 2l}{A(\tilde{r})} = \begin{bmatrix} \underset{l\times l}{0} & \underset{l\times l}{\tilde{r}I} \\ \underset{l\times l}{\frac{1}{\tilde{r}}K_r(\tilde{r})} & \underset{l\times l}{0} \end{bmatrix} \tag{A3}$$

$$\underset{2l\times 1}{\bar{r}(\tilde{r})} = \begin{bmatrix} \underset{l\times 1}{0} \\ \underset{l\times 1}{r(\tilde{r})} \end{bmatrix} \tag{A4}$$

Following the Peano-Baker form of integration (ref. 16), the solution of equation (A2) is

$$U(\tilde{r}) = \Omega_0^{\tilde{r}}(A)\ U(0)\ +\ \Omega_0^{\tilde{r}}(A)\ \int_0^{\tilde{r}} \left[\Omega_0^{\eta}(A)\right]^{-1} \bar{r}(\eta)\ d\eta \qquad (A5)$$

$$2l \times 1 \quad 2l \times 2l\ 2l \times 1 \quad 2l \times 2l \qquad 2l \times 2l\ \ 2l \times 1$$

where vector $U(0)$ consists of the boundary values of $(\tilde{r}\ \tilde{u})$ and $[1/\tilde{r}\ d/d\tilde{r}\ (\tilde{r}\ \tilde{u})]$ at the initial value of $\tilde{r}$ which is taken as zero in this case. The matrizant of $A(\tilde{r})$ is an infinite matrix integral series given by

$$\Omega_0^{\tilde{r}}(A) = I + \int_0^{\tilde{r}} A(\eta_1)\ d\eta_1 + \int_0^{\tilde{r}} A(\eta_2)\ d\eta_2 \int_0^{\eta_2} A(\eta_1)\ d\eta_1$$

$$+ \int_0^{\tilde{r}} A(\eta_3)\ d\eta_3 \int_0^{\eta_3} A(\eta_2)\ d\eta_2 \int_0^{\eta_2} A(\eta_1)\ d\eta_1 + \ldots \quad (A6)$$

Substituting matrix $A(\tilde{r})$ into equation (A6) leads to the following four matrix integral series in terms of the coefficient matrix $K(\tilde{r})$:

$$\Omega_{11}(\tilde{r}) = I + \int_0^{\tilde{r}} \eta_2\ I\ d\eta_2 \int_0^{\eta_2} \frac{1}{\eta_1} K_r(\eta_1)\ d\eta_1 + \ldots \quad (A7)$$

$$l \times l \quad l \times l \qquad\quad l \times l \qquad\quad l \times l$$

$$\Omega_{12}(\tilde{r}) = I \int_0^{\tilde{r}} \eta_1\ d\eta_1$$

$$l \times l \quad l \times l$$

$$+ \int_0^{\tilde{r}} I\ \eta_3\ d\eta_3 \int_0^{\eta_3} \frac{1}{\eta_2} K_r(\eta_2)d\eta_2 \int_0^{\eta_2} \eta_1\ I\ d\eta_1 + \ldots \quad (A8)$$

$$l \times l \qquad\quad l \times l \qquad\quad l \times l$$

30

$$\Omega_{21}(\tilde{r}) = \int_0^{\tilde{r}} \frac{1}{\eta_1} K_r(\eta_1)\, d\eta_1$$

$l \times l \qquad\qquad l \times l$

$$+ \int_0^{\tilde{r}} \frac{1}{\eta_3} K_r(\eta_3)\, d\eta_3 \int_0^{\eta_3} \eta_2\, I\, d\eta_2 \int_0^{\eta_2} \frac{1}{\eta_1} K_r(\eta_1)\, d\eta_1 + \ldots \tag{A9}$$

$l \times l \qquad\qquad l \times l \qquad\qquad l \times l$

$$\Omega_{22}(\tilde{r}) = I + \int_0^{\tilde{r}} \frac{1}{\eta_2} K_r(\eta_2)\, d\eta_2 \int_0^{\eta_2} \eta_1\, I\, d\eta_1 + \ldots \tag{A10}$$

$l \times l \quad l \times l \qquad\qquad l \times l \qquad\qquad l \times l$

An inspection of these equations shows that the following relations exist among these four matrix integral series:

$$\left.\begin{aligned}
\frac{1}{\tilde{r}} \frac{d\Omega_{11}(\tilde{r})}{d\tilde{r}} &= \Omega_{21}(\tilde{r}) \\[2ex]
\tilde{r}\, \frac{d\Omega_{21}(\tilde{r})}{d\tilde{r}} &= \Omega_{11}(\tilde{r}) K_r(\tilde{r})
\end{aligned}\right\} \tag{A11}$$

$$\left.\begin{aligned}
\frac{1}{\tilde{r}} \frac{d\Omega_{12}(\tilde{r})}{d\tilde{r}} &= \Omega_{22}(\tilde{r}) \\[2ex]
\tilde{r}\, \frac{d\Omega_{22}(\tilde{r})}{d\tilde{r}} &= \Omega_{12}(\tilde{r}) K_r(\tilde{r})
\end{aligned}\right\} \tag{A12}$$

From the definitions of these matrix series we can easily conclude that their initial values are

$$\left.\begin{array}{l} \Omega_{11}(\widetilde{r})\big|_{\widetilde{r}=0} = I \\[10pt] \Omega_{12}(\widetilde{r})\big|_{\widetilde{r}=0} = 0 \\[10pt] \Omega_{21}(\widetilde{r})\big|_{\widetilde{r}=0} = 0 \\[10pt] \Omega_{22}(\widetilde{r})\big|_{\widetilde{r}=0} = I \end{array}\right\} \qquad (A13)$$

Since the matrix series (A7) to (A10) are usually difficult to evaluate by performing the indicated integrations, the previous simultaneous matrix differential equations may be solved by a suitable numerical technique instead. The necessary initial conditions for these numerical solutions are given by equations (A13). For the examples presented in this report, the single step Runge-Kutta integration method was used to solve equations (A11) and (A12).

The particular integral of equation (A5) is written as

$$\begin{Bmatrix} B_1(\widetilde{r}) \\ l \times 1 \\ B_2(\widetilde{r}) \\ l \times 1 \end{Bmatrix} = \int_0^{\widetilde{r}} \begin{bmatrix} \Omega_{11}(\eta) & \Omega_{12}(\eta) \\ \Omega_{21}(\eta) & \Omega_{22}(\eta) \end{bmatrix}^{-1} \begin{Bmatrix} 0 \\ r(\eta) \end{Bmatrix} d\eta \qquad (A14)$$

In evaluating the inverse of Ω by partitioning, the partitioned integrals (A14) are given by

$$B_1(\widetilde{r}) = - \int_0^{\widetilde{r}} \Omega_{11}\Omega_{12}(\Omega_{22} - \Omega_{21}\Omega_{11}\Omega_{12})^{-1} r(\eta) \, d\eta \qquad (A15)$$

$$B_2(\widetilde{r}) = \int_0^{\widetilde{r}} \left(\Omega_{22} - \Omega_{21}\Omega_{11}^{-1}\Omega_{12}\right)^{-1} r(\eta) \, d\eta \qquad (A16)$$

If it is assumed that $r(\eta)$ is known, the previous particular integrals can easily be evaluated. When the partitioned form of the matrices is used, equation (A5) may be written as

32

$$\left\{ \begin{array}{c} \tilde{r}\,\tilde{u} \\[2ex] \dfrac{1}{\tilde{r}}\dfrac{d}{d\tilde{r}}(\tilde{r}\,\tilde{u}) \end{array} \right\} = \begin{bmatrix} \Omega_{11}(\tilde{r}) & \Omega_{12}(\tilde{r}) \\[2ex] \Omega_{21}(\tilde{r}) & \Omega_{22}(\tilde{r}) \end{bmatrix} \left(\left\{ \begin{array}{c} \tilde{r}\,\tilde{u} \\[2ex] \dfrac{1}{\tilde{r}}\dfrac{1}{d\tilde{r}}(\tilde{r}\,\tilde{u}) \end{array} \right\}_{\tilde{r}=0} + \left\{ \begin{array}{c} B_1(\tilde{r}) \\[2ex] B_2(\tilde{r}) \end{array} \right\} \right) \tag{A17}$$

from which the solution vectors (18) and (21) can be directly constructed.

It may be noted that for axisymmetric problems the following identities can be used to evaluate the particular integrals:

$$\left. \begin{array}{l} \Omega_{11} = \left(\Omega_{22} - \Omega_{21}\Omega_{11}^{-1}\Omega_{12} \right)^{-1} \\[3ex] \Omega_{12} = \Omega_{11}\Omega_{12}\left(\Omega_{22} - \Omega_{21}\Omega_{11}^{-1}\Omega_{12} \right)^{-1} \end{array} \right\} \tag{A18}$$

These identities are obtained from noting that the inverse of the matrizant $\Omega_0^{\tilde{r}}(A)$ is given by

$$\begin{pmatrix} \Omega_{11} & \Omega_{12} \\[2ex] \Omega_{21} & \Omega_{22} \end{pmatrix}^{-1} = \begin{pmatrix} \Omega_{22} & -\Omega_{12} \\[2ex] -\Omega_{21} & \Omega_{11} \end{pmatrix} \tag{A19}$$

when the coefficient matrix is of the form (A3) and the matrix K_r has constants for its elements.

33

APPENDIX B

SOLUTION OF SIMULTANEOUS DIFFERENTIAL EQUATIONS

WITH CONSTANT COEFFICIENTS

For the solution of equations (16) we introduce the following new variables:

$$
\left.
\begin{aligned}
V_1 = \tilde{v}_1,\ V_2 = \tilde{v}_2,\ \ldots,\ V_m = \tilde{v}_m \\[2mm]
V_{m+1} = \frac{d\tilde{v}_1}{d\tilde{\theta}},\ V_{m+2} = \frac{d\tilde{v}_2}{d\tilde{\theta}},\ \ldots,\ V_{2m} = \frac{d\tilde{v}_m}{d\tilde{\theta}}
\end{aligned}
\right\}
\qquad \text{(B1)}
$$

In terms of these variables, equations (16) can be written as a set of first-order differential equations. Hence, we have

$$
\frac{dV}{d\tilde{\theta}} = A_\theta \quad V \quad + \quad \overline{s}(\tilde{\theta}) \qquad \text{(B2)}
$$

$$
2m \times 1 \quad 2m \times 2m \quad 2m \times 1 \quad 2m \times 1
$$

where

$$
\begin{array}{c}
A_\theta \\
2m \times 2m
\end{array}
=
\begin{bmatrix}
\underset{m \times m}{0} & \underset{m \times m}{I} \\[3mm]
\underset{m \times m}{K_\theta} & \underset{m \times m}{0}
\end{bmatrix}
\qquad \text{(B3)}
$$

$$
\begin{array}{c}
\overline{s}(\tilde{\theta}) \\
2m \times 1
\end{array}
=
\left\{
\begin{array}{c}
0 \\
m \times 1 \\[3mm]
s(\tilde{\theta}) \\
m \times 1
\end{array}
\right\}
\qquad \text{(B4)}
$$

34

The solution of equation (B2) is well known and can be written as (ref. 16)

$$V(\tilde{\theta}) = e^{A\tilde{\theta}} \quad V(0) + e^{A\tilde{\theta}} \int_0^{\tilde{\theta}} e^{-A\eta} \quad \bar{s}(\eta) \ d\eta \tag{B5}$$

$$2m \times 1 \quad 2m \times 2m \ 2m \times 1 \ 2m \times 2m \qquad 2m \times 2m \ 2m \times 1$$

where $V(0)$ is an initial value vector whose evaluation from given boundary conditions is discussed in appendix C and $e^{A\tilde{\theta}}$ is a matrix series given by

$$e^{A\tilde{\theta}} = I + \frac{A\tilde{\theta}}{1!} + \frac{A^2\tilde{\theta}^2}{2!} + \frac{A^3\tilde{\theta}^3}{3!} + \ldots \tag{B6}$$

In terms of the coefficient matrix K_θ, equation (B6) yields

$$e^{A\tilde{\theta}} = \begin{bmatrix} \displaystyle\sum_{i=0}^{\infty} \frac{\tilde{\theta}^{2i}}{(2i)!} K_\theta^i & \displaystyle\sum_{i=0}^{\infty} \frac{\tilde{\theta}^{2i+1}}{(2i+1)!} K_\theta^i \\[2em] \displaystyle\sum_{i=0}^{\infty} \frac{\tilde{\theta}^{2i+1}}{(2i+1)!} K_\theta^{i+1} & \displaystyle\sum_{i=0}^{\infty} \frac{\tilde{\theta}^{2i}}{(2i)!} K_\theta^i \end{bmatrix} \tag{B7}$$

$$e^{A\tilde{\theta}} \atop 2m \times 2m = \begin{bmatrix} A_{11}(\tilde{\theta}) & A_{12}(\tilde{\theta}) \\ m \times m & m \times m \\ A_{21}(\tilde{\theta}) & A_{22}(\tilde{\theta}) \\ m \times m & m \times m \end{bmatrix} \tag{B8}$$

From equations (B7) and (B8) we note that

$$A_{11}(\tilde{\theta}) = A_{22}(\tilde{\theta}) = \cosh K_\theta^{1/2}\tilde{\theta} \tag{B9}$$

$$A_{12}(\tilde{\theta}) = K_\theta^{-1/2} \sinh K_\theta^{1/2}\tilde{\theta} \tag{B10}$$

35

$$A_{21}(\tilde{\theta}) = K_\theta A_{12}(\tilde{\theta}) \tag{B11}$$

where $K_\theta^{1/2}$ is a matrix whose square is equal to K_θ. Noting that A_{11} and A_{22} are even functions of $\tilde{\theta}$ while A_{12} and A_{21} are odd functions of $\tilde{\theta}$, the inverse of $e^{A\tilde{\theta}}$ becomes

$$e^{-A\tilde{\theta}} = \begin{bmatrix} A_{11}(\tilde{\theta}) & -A_{12}(\tilde{\theta}) \\ -A_{21}(\tilde{\theta}) & A_{22}(\tilde{\theta}) \end{bmatrix} \tag{B12}$$

Substituting equations (B8) and (B12) into the identity of $e^{A\tilde{\theta}} \cdot e^{-A\tilde{\theta}} = I$ yields

$$A_{11}^2(\tilde{\theta}) - K_\theta \; A_{12}^2(\tilde{\theta}) = I \tag{B13}$$
$$\underset{m \times m}{} \quad \underset{m \times m}{} \underset{m \times m}{} \quad \underset{m \times m}{}$$

Matrix functions (B9) and (B10) may be evaluated for each value of the independent variable from the series definitions given in equation (B7). The truncation point in each series is determined by the required accuracy for the convergence of the successive approximation calculations. Equation (B13) may be used as a measure of this required accuracy. However, for increasing values of $\tilde{\theta}$ serious convergence difficulties may arise and an impractically large number of terms must be calculated. In order to avoid these computational difficulties, additive formulas for these matrix functions may be obtained from using the identity of

$$e^{A\tilde{\theta}_1} \cdot e^{A\tilde{\theta}_2} = e^{A(\tilde{\theta}_1 + \tilde{\theta}_2)} \tag{B14}$$

In terms of the submatrices $A_{ij}(\tilde{\theta})$, this identity yields the following equations:

$$A_{11}(\tilde{\theta}_1 + \tilde{\theta}_2) = A_{11}(\tilde{\theta}_1)A_{11}(\tilde{\theta}_2) + A_{21}(\tilde{\theta}_1)A_{12}(\tilde{\theta}_2) \tag{B15}$$

$$A_{12}(\tilde{\theta}_1 + \tilde{\theta}_2) = A_{12}(\tilde{\theta}_1)A_{11}(\tilde{\theta}_2) + A_{11}(\tilde{\theta}_1)A_{12}(\tilde{\theta}_2) \tag{B16}$$

The advantage of using equations (B7), (B15), and (B16) is that the solution of an eigen-value problem is not required. Alternate methods for the evaluation of these matrix functions using the solution of the determinantal equation are discussed in reference 6.

The particular integrals of equations (16) are constructed in a similar manner to

36

those listed in equations (A15) and (A16). The analogous particular integrals are

$$B_3(\tilde{\theta}) = - \int_0^{\tilde{\theta}} A_{12}(\eta) \ s(\eta) \ d\eta \qquad (B17)$$

$$m \times 1 \qquad m \times m \ m \times 1$$

$$B_4(\tilde{\theta}) = \int_0^{\tilde{\theta}} A_{11}(\tilde{\theta}) \ s(\eta) \ d\eta \qquad (B18)$$

$$m \times 1 \qquad m \times m \ m \times 1$$

Assuming that $s(\eta)$ is known, these integrals can easily be evaluated. When the partitioned form of the matrices is used, solution vector (B5) for the circumferential differential equations may be written as

$$\begin{Bmatrix} \tilde{v}(\tilde{\theta}) \\ \dot{\tilde{v}}(\tilde{\theta}) \end{Bmatrix} = \begin{bmatrix} A_{11}(\tilde{\theta}) & A_{12}(\tilde{\theta}) \\ A_{21}(\tilde{\theta}) & A_{22}(\tilde{\theta}) \end{bmatrix} \left(\begin{Bmatrix} \tilde{v}(0) \\ \dot{\tilde{v}}(0) \end{Bmatrix} + \begin{Bmatrix} B_3(\tilde{\theta}) \\ B_4(\tilde{\theta}) \end{Bmatrix} \right) \qquad (B19)$$

which when expanded yields equations (22) and (27).

APPENDIX C

DEVELOPMENT OF INITIAL VALUE VECTORS

Since the problems discussed in this report are two point boundary value problems, the initial values of both the displacements and their derivatives are usually not available. As an example of how to obtain these initial values from given boundary conditions, consider the problem of figure 2 in more detail.

From the definition of vector F_1 and the symmetry of the problem, we can immediately conclude that

$$F_1 = \tilde{r}\,\tilde{u}\,\big|_{\tilde{r}=0} = 0 \tag{C1}$$
$$l \times 1$$

The zero normal stress boundary condition on the surface $\tilde{r} = \tilde{b}$ will be used in conjunction with equation (C1) to evaluate the vector F_2 for this problem. Using equation (5) gives

$$\dot{\tilde{u}}\,\big|_{\tilde{r}=\tilde{b}} = -\frac{\lambda}{\lambda + 2G}\left(\frac{\tilde{u}}{\tilde{b}} + \dot{\tilde{w}}\right)_{\tilde{r}=\tilde{b}} \tag{C2}$$

Equation (18), taken at $\tilde{r} = \tilde{b}$, can be used to eliminate the vector $\tilde{u}\,\big|_{\tilde{r}=\tilde{b}}$ in equation (C2). The resulting equation for the vector $\dot{\tilde{u}}\,\big|_{\tilde{r}=\tilde{b}}$ can then be substituted into equation (21), which is also evaluated at $\tilde{r} = \tilde{b}$, to find the vector F_2. The results of these manipulations are

$$F_2 = \frac{\lambda}{\lambda + 2G}\,\Omega_b^{-1}\,\dot{\tilde{w}}\,\big|_{\tilde{r}=\tilde{b}} - \Omega_b^{-1}\Omega_a B_1(\tilde{b}) - B_2(\tilde{b}) \tag{C3}$$

where

$$\Omega_a = \frac{2G}{(\lambda + 2G)\tilde{b}^2}\,\Omega_{11}(\tilde{b}) - \Omega_{11}(\tilde{b}) \tag{C4}$$

$$\Omega_b = \frac{2G}{(\lambda + 2G)\tilde{b}^2}\,\Omega_{12}(\tilde{b}) - \Omega_{22}(\tilde{b}) \tag{C5}$$

Note that by using L'Hospital's rule as $\tilde{r} \to 0$ the solution vectors (18) and (21) for the

38

problem in figure 2 become

$$\left.\begin{array}{l} \tilde{u}(0) = 0 \\[2mm] \dot{\tilde{u}}(0) = \dfrac{F_2}{2} \end{array}\right\} \tag{C6}$$

Since for axisymmetric problems the circumferential displacements are inherently zero, the initial value vectors of the axial solutions will be considered next. An analogous solution to equations (22) and (27) along the z-directional lines can be written as

$$\left\{\begin{array}{c} \tilde{w}(\tilde{z}) \\[2mm] \dot{\tilde{w}}(\tilde{z}) \end{array}\right\} = \begin{bmatrix} A_{11}(\tilde{z}) & A_{12}(\tilde{z}) \\[2mm] A_{21}(\tilde{z}) & A_{22}(\tilde{z}) \end{bmatrix} \left(\left\{\begin{array}{c} \tilde{w}(0) \\[2mm] \dot{\tilde{w}}(0) \end{array}\right\} + \left\{\begin{array}{c} B_5(\tilde{z}) \\[2mm] B_6(\tilde{z}) \end{array}\right\}\right) \tag{C7}$$

If the number of axial lines falling over the crack surface is denoted as NIC and those falling outside as NOC, the zero normal stress condition over the crack face and the symmetry condition in the crack plane result in the following equations:

$$\dot{\tilde{w}}(0) = \frac{-\lambda}{\lambda + 2G}\left(\dot{\tilde{u}} + \frac{\tilde{u}}{\tilde{r}}\right)_{\tilde{z}=0} \tag{C8}$$

NIC × 1   inside crack

$$\tilde{w}(0) = 0\Big|_{\tilde{z}=0} \tag{C9}$$

NOC × 1   outside crack

Assuming that on the face $\tilde{z} = \tilde{L}$ we have a uniform tensile stress of σ_0 as shown in figure 2, the normal stress boundary condition on this plane gives

$$\dot{\tilde{w}}(\tilde{L}) = \frac{\sigma_0}{\lambda + 2G} - \frac{\lambda}{\lambda + 2G}\left(\dot{\tilde{u}} + \frac{\tilde{u}}{\tilde{r}}\right)_{\tilde{r}=\tilde{L}} \tag{C10}$$

n × 1

This vector can be suitably partitioned into vectors $\dot{\tilde{w}}_\alpha(\tilde{L})$ and $\dot{\tilde{w}}_\beta(\tilde{L})$. For convenience of matrix manipulations, we construct the vectors as follows:

NIC × 1   NOC × 1

$$\begin{Bmatrix} \tilde{w}(0) \\ n \times 1 \\ \dot{\tilde{w}}(0) \\ n \times 1 \end{Bmatrix} = \begin{Bmatrix} F_5 \\ F_6 \end{Bmatrix} = \begin{Bmatrix} F_{5\alpha} \\ NIC \times 1 \\ F_{5\beta} \\ NOC \times 1 \\ F_{6\alpha} \\ NIC \times 1 \\ F_{6\beta} \\ NOC \times 1 \end{Bmatrix} \qquad (C11)$$

Values of $F_{6\alpha}$ and $F_{5\beta}$ are given by equations (C8) and (C9), respectively. From equation (C7) we can express $\tilde{w}(\tilde{L})$ in a partitioned form consistent with equation (C11) as

$$\begin{Bmatrix} \dot{\tilde{w}}_\alpha \\ NIC \times 1 \\ \dot{\tilde{w}}_\beta \\ NOC \times 1 \end{Bmatrix}_{\tilde{z}=\tilde{L}} = \begin{bmatrix} A_{21\alpha 1} & A_{21\alpha 2} \\ NIC \times NIC & NIC \times NOC \\ A_{21\beta 1} & A_{21\beta 2} \\ NOC \times NIC & NOC \times NOC \end{bmatrix}_{\tilde{z}=\tilde{L}} \left(\begin{Bmatrix} F_{5\alpha} \\ NIC \times 1 \\ F_{5\beta} \\ NOC \times 1 \end{Bmatrix} + \begin{Bmatrix} B_{5\alpha} \\ NIC \times 1 \\ B_{5\beta} \\ NOC \times 1 \end{Bmatrix}_{\tilde{z}=\tilde{L}} \right)$$

$$+ \begin{bmatrix} A_{22\alpha 1} & A_{22\alpha 2} \\ NIC \times NIC & NIC \times NOC \\ A_{22\beta 1} & A_{22\beta 2} \\ NOC \times NIC & NOC \times NOC \end{bmatrix}_{\tilde{z}=\tilde{L}} \left(\begin{Bmatrix} F_{6\alpha} \\ NIC \times 1 \\ F_{6\beta} \\ NOC \times 1 \end{Bmatrix} + \begin{Bmatrix} B_{6\alpha} \\ NIC \times 1 \\ B_{6\beta} \\ NOC \times 1 \end{Bmatrix}_{\tilde{z}=\tilde{L}} \right)$$

$$(C12)$$

Equation (C12) leads to two matrix equations involving the two unknown vectors $F_{5\alpha}$ and $F_{6\beta}$. A solution of these equations yields

$$F_{6\beta} = \frac{1}{\lambda + 2G} \left[A_a^{-1} \quad \sigma_{0\beta} - \lambda \quad A_a^{-1} \left(\dot{\tilde{u}}_\beta + \frac{\tilde{u}_\beta}{\tilde{r}} \right)_{\tilde{z} = \tilde{L}} \right]$$

NOC × 1   NOC × NOC NOC × 1   NOC × NOC NOC × 1   NOC × 1

$$- \frac{1}{\lambda + 2G} \left[A_a^{-1} \quad A_{21\beta1} \quad A_{21\alpha1}^{-1} \quad \sigma_{0\alpha} \right.$$

NOC × NOC NOC × NIC NIC × NIC NIC × 1

$$\left. - \lambda \quad A_a^{-1} \quad A_{21\beta1} \quad A_{21\alpha1}^{-1} \left(\dot{\tilde{u}}_\alpha + \frac{\tilde{u}_\alpha}{\tilde{r}} \right)_{\tilde{z} = \tilde{L}} \right]$$

NOC × NOC NOC × NIC NIC × NIC NIC × 1   NIC × 1

$$- A_a^{-1} \quad A_b \quad B_{5\beta}(\tilde{L}) - A_a^{-1} \quad A_c \quad B_{6\alpha}(\tilde{L})$$

NOC × NOC NOC × NOC NOC × 1   NOC × NOC NOC × NIC NIC × 1

$$- B_{6\beta}(\tilde{L}) + \frac{\lambda}{\lambda + 2G} \quad A_a^{-1} \quad A_c \left(\dot{\tilde{u}}_\alpha + \frac{\tilde{u}_\alpha}{\tilde{r}} \right)_{\tilde{z} = 0}$$

NOC × 1   NOC × NOC NOC × NIC NIC × 1   NIC × 1

(C13)

where

$$A_a = \left(A_{22\beta2} - A_{21\beta1} \quad A_{21\alpha1}^{-1} \quad A_{22\alpha2} \right)_{\tilde{z} = \tilde{L}} \qquad (C14)$$

NOC × NOC   NOC × NOC   NOC × NIC NIC × NIC NIC × NOC

$$A_b = \left(A_{21\beta2} - A_{21\beta1} \quad A_{21\alpha1}^{-1} \quad A_{21\alpha2} \right)_{\tilde{z} = \tilde{L}} \qquad (C15)$$

NOC × NOC   NOC × NOC   NOC × NIC NIC × NIC NIC × NOC

$$A_c = \left(A_{22\beta1} - A_{21\beta1} \quad A_{21\alpha1}^{-1} \quad A_{22\alpha1} \right)_{\tilde{z} = \tilde{L}} \qquad (C16)$$

NOC × NIC   NOC × NIC   NOC × NIC NIC × NIC NIC × NIC

Note that the particular integrals, the applied stress vector, and the radial displacements and their derivatives are also partitioned according to their location with respect

to the crack.

The crack opening displacement is given by

$$
F_{5\alpha} = \frac{1}{\lambda + 2G}\left[A_{21\alpha1}^{-1} \quad \sigma_{0\alpha} - \lambda \; A_{21\alpha1}^{-1}\left(\dot{\tilde{u}}_\alpha + \frac{\tilde{u}_\alpha}{\tilde{r}} \right)_{\tilde{z}=\tilde{L}} \right.
$$

NIC × 1   NIC × NIC   NIC × 1   NIC × NIC   NIC × 1   NIC × 1

$$
- B_{5\alpha}(\tilde{L}) - A_{21\alpha1}^{-1} \quad A_{21\alpha2} \quad B_{5\beta}(\tilde{L}) - A_{21\alpha1}^{-1} \quad A_{22\alpha2} \quad B_{6\alpha}(\tilde{L})
$$

NIC × 1   NIC × NIC   NIC × NOC   NOC × 1   NIC × NIC   NIC × NIC   NIC × 1

$$
+ \frac{\lambda}{\lambda + 2G} \; A_{21\alpha1}^{-1} \quad A_{22\alpha1} \left(\dot{\tilde{u}}_\alpha + \frac{\tilde{u}_\alpha}{\tilde{r}} \right)_{\tilde{z}=0}
$$

NIC × NIC   NIC × NIC   NIC × 1   NIC × 1

$$
- A_{21\alpha1}^{-1} \quad A_{22\alpha2} \quad F_{6\beta} - A_{21\alpha1}^{-1} \quad A_{22\alpha2} \quad B_{6\beta}(\tilde{L}) \qquad (C17)
$$

NIC × NIC   NIC × NOC   NOC × 1   NIC × NIC   NIC × NOC   NOC × 1

where $F_{6\beta}$ is given by equation (C13). Although the matrix $A_{21}(\tilde{L})$ is singular, the partitioned matrices are not. In calculating the previous equations the indeterminate terms at $\tilde{r} = 0$ must be carefully considered.

REFERENCES

1. Lur'e, A. I.: Three-Dimensional Problems of the Theory of Elasticity. Interscience Publishers, 1964.

2. Ayres, David J.: A Numerical Procedure for Calculating Stress and Deformation Near a Slit in a Three-Dimensional Elastic-Plastic Solid. NASA TM X-52440, 1968.

3. Cruse, T. A.: The Direct Potential Method in Three-Dimensional Elastostatics. Rep. SM-13, Carnegie-Mellon University (NASA CR-66673), June 1968.

4. Zienkiewicz, Olgierd C.: The Finite Element Method in Engineering Science. Second ed., McGraw-Hill Book Co., Inc., 1971.

5. Hartranft, R. J.; and Sih, G. C.: The Use of Eigenfunction Expansions in the General Solution of Three-Dimensional Crack Problems. J. Math. Mech., vol. 19, no. 2, Aug. 1969, pp. 123-138.

6. Gyekenyesi, John P.: Solution of Some Mixed Boundary Value Problems of Three-Dimensional Elasticity by the Method of Lines. Ph.D. Thesis, Michigan State Univ., 1972.

7. Faddeeva, V. N.: The Method of Lines Applicable to Some Boundary Problems. Trudy Mat. Inst. Steklov, vol. 28, 1949, pp. 73-103.

8. Irobe, Makoto: Method of Numerical Analysis for Three-Dimensional Elastic Problems. Proceedings of the 16th Japan National Congress of Applied Mechanics. Central Scientific Publishers, Tokyo, 1968, pp. 1-7.

9. Sneddon, I. N.: The Distribution of Stress in the Neighbourhood of a Crack in an Elastic Solid. Proc. Roy. Soc. (London), Ser. A, vol. 187, no. 1009, Oct. 22, 1946, pp. 229-260.

10. Hartranft, R. J.; and Sih, G. C.: An Approximate Three-Dimensional Theory of Plates with Application to Crack Problems. Tech. Rep. 7, Lehigh Univ. (NASA CR-103211), May 1968.

11. Cruse, T. A.; and Van Buren, W.: Three-Dimensional Elastic Stress Analysis of a Fracture Specimen with an Edge Crack. Rep. SM-21, Carnegie-Mellon University, Dept. of Mech. Eng., January 1970.

12. Gyekenyesi, John P.; Mendelson, Alexander; and Kring, Jon: Three-Dimensional Elastic Stress and Displacement Analysis of Tensile Fracture Specimens Containing Cracks. NASA TN D-7213, 1973.

13. Sneddon, I. N.; and Welch, J. T.: A Note on the Distribution of Stress in a Cylinder Containing a Penny-Shaped Crack. Int. J. Eng. Sci., vol. 1, 1963, pp. 411-419.

14. Paris, P. C.; and Sih, G. C.: Stress Analysis of Cracks. Fracture Toughness Testing and Its Applications. Spec. Tech. Publ. No. 381, ASTM, 1965, pp. 30-83.

15. Sneddon, I. N.: Crack Problems in the Mathematical Theory of Elasticity. North Carolina State College, Dept. of Mathematics and Eng. Res., 1961.

16. Frazer, R. A.; Duncan, W. J.; and Collar, A. R.: Elementary Matrices and Some Applications to Dynamics and Differential Equations. Cambridge University Press, 1938.

Page Intentionally Left Blank

"The aeronautical and space activities of the United States shall be conducted so as to contribute . . . to the expansion of human knowledge of phenomena in the atmosphere and space. The Administration shall provide for the widest practicable and appropriate dissemination of information concerning its activities and the results thereof."
—NATIONAL AERONAUTICS AND SPACE ACT OF 1958

NASA SCIENTIFIC AND TECHNICAL PUBLICATIONS

TECHNICAL REPORTS: Scientific and technical information considered important, complete, and a lasting contribution to existing knowledge.

TECHNICAL NOTES: Information less broad in scope but nevertheless of importance as a contribution to existing knowledge.

TECHNICAL MEMORANDUMS: Information receiving limited distribution because of preliminary data, security classification, or other reasons. Also includes conference proceedings with either limited or unlimited distribution.

CONTRACTOR REPORTS: Scientific and technical information generated under a NASA contract or grant and considered an important contribution to existing knowledge.

TECHNICAL TRANSLATIONS: Information published in a foreign language considered to merit NASA distribution in English.

SPECIAL PUBLICATIONS: Information derived from or of value to NASA activities. Publications include final reports of major projects, monographs, data compilations, handbooks, sourcebooks, and special bibliographies.

TECHNOLOGY UTILIZATION PUBLICATIONS: Information on technology used by NASA that may be of particular interest in commercial and other non-aerospace applications. Publications include Tech Briefs, Technology Utilization Reports and Technology Surveys.

Details on the availability of these publications may be obtained from:

SCIENTIFIC AND TECHNICAL INFORMATION OFFICE

NATIONAL AERONAUTICS AND SPACE ADMINISTRATION
Washington, D.C. 20546